INRIA

INSTITUT NATIONAL DE RECHERCHE EN INFORMATIQUE ET EN AUTOMATIQUE

A General Scheme for Automatically Building 3D Morphometric Anatomical Atlases: application to a Skull Atlas

Gérard Subsol, Jean-Philippe Thirion, Nicholas Ayache

N° 2586

Mai 1995

PROGRAMME 4

ISSN 0249-6399

INRIA
SOPHIA ANTIPOLIS

A General Scheme for Automatically Building 3D Morphometric Anatomical Atlases: application to a Skull Atlas

Gérard Subsol*, Jean-Philippe Thirion**, Nicholas Ayache***

Programme 4 — Robotique, image et vision
Projet Epidaure

Rapport de recherche n ° 2586 — Mai 1995 — 35 pages

Abstract: In this research report, we present a general scheme for building entirely automatically a morphometric anatomical atlas from 3D medical images (CT-Scan, Magnetic Resonance Imagery). We detail each step of the method, including the non-rigid registration algorithm, 3D feature lines averaging, and statistical processes.

We apply the method to obtain a quantitative atlas of crest lines of the skull. Finally, we use the resulting atlas to study a craniofacial disease: we show how we can obtain qualitative and quantitative medical results by contrasting a skull affected by Crouzon's disease with the atlas.

Key-words: electronic anatomical atlas, crest lines, non-rigid registration, shape analysis, automatic medical diagnosis, skull, morphometry, computer aided surgery.

(Résumé : tsvp)

*Gerard.Subsol@epidaure.inria.fr
**Jean-Philippe.Thirion@epidaure.inria.fr
***Nicholas.Ayache@epidaure.inria.fr

Unité de recherche INRIA Sophia-Antipolis
2004 route des Lucioles, BP 93, 06902 SOPHIA-ANTIPOLIS Cedex (France)
Téléphone : (33) 93 65 77 77 – Télécopie : (33) 93 65 77 65

Une méthode générale pour construire automatiquement des atlas anatomiques morphométriques : application a un atlas du crâne

Résumé : Dans ce rapport, nous présentons une méthode générale pour construire de manière automatique des atlas anatomiques morphométriques à partir d'images médicales tridimensionnelles (obtenues par scannographie ou Imagerie par Résonance Magnétique). Nous détaillons les étapes de la méthode, en particulier, les algorithmes de mise en correspondance non-rigide, de moyenne de lignes caractéristiques tridimensionnelles et d'analyse statistique.

Nous appliquons la méthode à la construction d'un atlas quantitatif des lignes de crête du crâne. Nous utilisons alors l'atlas pour étudier des difformités craniofaciales ; nous montrons comment la comparaison entre l'atlas et un crâne déformé par la maladie de Crouzon permet d'obtenir des résultats qualitatifs et quantitatifs utilisables par un médecin.

Mots-clé : atlas anatomique informatique, lignes de crête, mise en correspondance non-rigide, analyse de la forme, diagnostic médical automatique, crâne, morphométrie, chirurgie assistée par ordinateur.

1 Introduction

In order to improve diagnosis and therapy planning, a physician needs to compare 3D medical images coming from Computed Tomography, Magnetic Resonance Imagery or Nuclear Medicine. We can distinguish between three kinds of comparison: comparison of images of the same patient to study the evolution of a disease, comparison of images of different patients to contrast a healthy and a pathological person, and registration of images with an electronic anatomical atlas.

1.1 Description of the problem

How do we define an electronic anatomical atlas? Let us assume that we have a database of 3D medical images of "normal" patients, for example the 6 skulls called $\mathcal{A}$ to $\mathcal{F}$ displayed in Figure 1.

A skull atlas, based on this database, has to take into account the resemblances as the diversity of the 6 skulls to constitute a set of *features* which are anatomically meaningful. Figure 2 is what we want to obtain, an "average" skull built according to the general scheme described in the present paper.

Over the past few years, many electronic anatomical atlases based on 3D medical images have been developed, widening or opening new fields of medical applications.

1.2 Applications of electronic anatomical atlases

- 1) *reference database*: the practitioners refer to the electronic atlas for consulting and teaching. Thus, Voxel-Man atlas [HBR+92] include powerful volume visualization techniques to display anatomical structures according to any point of view with functionalities such as cutting or transparency. To improve the accuracy of the description, multi-level atlases have been proposed as presented in [NFN+95]. It is also possible to couple these atlases with a knowledge database to represent and manage the anatomy [PSR+94] [BGM+94] and functional information [Nig90].

- 2) *normalized registration*: in order to locate anatomical structures and detect abnormalities, the atlas and the patient data must be registered.

Figure 1: The skulls $\mathcal{A}$, $\mathcal{B}$, $\mathcal{C}$, $\mathcal{D}$, $\mathcal{E}$, $\mathcal{F}$. These skulls were segmented from very precise CT-Scan images (acquired from two different devices, the voxel size is about $1mm \times 1mm \times 1.5mm$) by classic mathematical morphology and thresholding tools. We can notice a quite important diversity in the skull size and shape.

In a first time, the process can be manual. For example, in [SHC+94], the user specifies manually some landmarks in the patient data and a linear transformation based on the Talairach method, is computed, superimposing the Voxel-Man brain atlas to patient data. In [MDB+94], a Talairach proportional localization system based on two external markers and some manually detected landmarks is used for brain SPECT images. In [MECP89], a more complex method is proposed to register an atlas with MRI data: after a global affine matching is performed manually, the user can choose a (or a set of) volume of interest in order to apply a locally affine transformation. [GBHE91] introduced quadratic transfor-

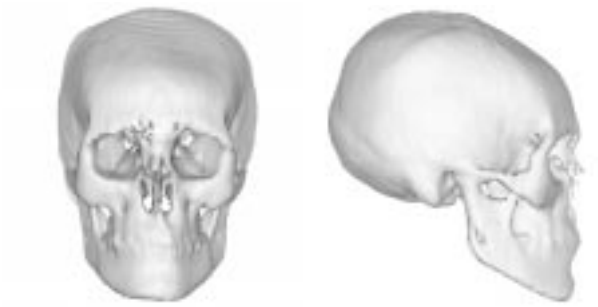

Figure 2: *The skull atlas obtained by the general scheme described in the report.*

mations (called pear, skew, asymmetry or scoliosis) besides linear ones (translation, rotation, scalings) in their Computerized Brain Atlas.

The first automatic registration method was introduced in [BK89] to find the cortical and ventricle structures. It relies on a global rigid matching based on a principal axis and elastic matching with external forces based on a local similarity measure. This method is evaluated in [GRB93]. In [CMV94], the authors adopt a Bayesian approach to estimate the deformation field and have implemented the algorithm on a massively-parallel computer.

- 3) *passive aided surgery*: it is passive in the sense that the computer aids the surgeon by displaying useful information but does not intervene in the diagnosis or surgery process itself.

  If atlas visualization and registration are added to a surgery simulation program (craniofacial surgery [DSCP94] or stereotactic surgery [Har94]), the user can manipulate more easily the patient data thanks to automatic labeling and to contrast the patient data with the normalized atlas. A medical doctor can then plan surgical procedures.

  Moreover, if the registration algorithm can work in real time (at least, a frequency of several hertz), it becomes possible to superimpose the visualization of the atlas on the real image of the surgery. This is the

principle of "enhanced reality" developed by several teams [GLPWI+94], [BFAD95] and [CZH+94].

- 4) *shape and deformation analysis*: the aim is to obtain morphometric parameters (morphometry is "the study of covariances of biological form" [Boo91]).

  Then, one can create a "virtual patient" i.e. a normalized model of a patient built from an atlas that is deformed towards pathologic cases according to the precomputed deformations characterizing a given disease.

- 5) *automatic diagnosis*: quantitative results may lead to automatic diagnosis. After the registration between the morphometric atlas and the patient data, a statistical analysis of the features can be performed. Some features considered "abnormal" become symptoms. Coupled with an expert system, for example proposed by [SYMK95], the "abnormal" anatomical structures are automatically pointed out.

- 6) *automatic surgery*: by combining automatic diagnosis and path planning in the atlas, it is possible to automate some stages of surgery or radiotherapy [LTG+92] [Tay93] [TSLA95] [OISJ+95].

Nevertheless, current electronic atlases have two main drawbacks that prevent them actually being used in applications 4, 5 and 6.

1.3 Current limitations

- *lack of accuracy*: electronic atlases are basically built manually (with some semi-automatic tools): 3D medical images are segmented by anatomy specialists slice-by-slice according to paper atlases [Per83]. This process is extremely tedious and long (several hours for the 150 slices of the skull images of figure 1). But, how to deal with the tremendous precision of new medical imaging devices (voxel size smaller than 1 mm) whereas paper atlas are much less accurate as well as being quite hard to read? How to interpolate between the pages of the paper atlas in order to ensure 3D consistency of the electronic version? All these factors reduce the accuracy of electronic atlases.

Moreover, the registration between the atlas and the patient data is in general manual. Therefore, if one can deal with 3D affine transformations as in the Talairach reference frame or even 3D quadratic transformations, it is not sufficient to obtain a precise and useful registration.

- *lack of quantitative data* such as feature position or feature deviation analysis. It is not always possible to identify manually with high precision the features in the huge 3D medical images and then compute their coordinates and useful statistics.

  Moreover, electronic atlases are often based on one, or a very reduced set of, patients whereas significant statistic results can only be obtained with a suitably large set of data.

We conclude that only automatic tools can allow the building of anatomical atlas taking into account the accuracy of new medical images and including quantitative data. We propose in the following a general scheme to achieve this task. Some similar work can be found in [CBH+93] concerning the building of a skull atlas and in [BBW+94] concerning a "normalized geometric liver", both of them based on statistics methods introduced by Bookstein, and also in [MFB+94] concerning the cortex topography.

2 The general scheme

Our general scheme is composed of five steps (see Figure 3):

- Step 1: *feature extraction*. This step consists of automatically extracting the anatomically meaningful features in the images. One needs to choose a feature type which combines a mathematical definition in order to be automatically computed and anatomical relevance in order to constitute a meaningful atlas.
- Step 2: *features registration*. We find correspondences between the sets of features by using a non-rigid registration algorithm.
- Step 3: *common feature subset extraction*. After registration, we identify which features are common to all the data sets. These common feature subsets will form the *topological structure* of the atlas.

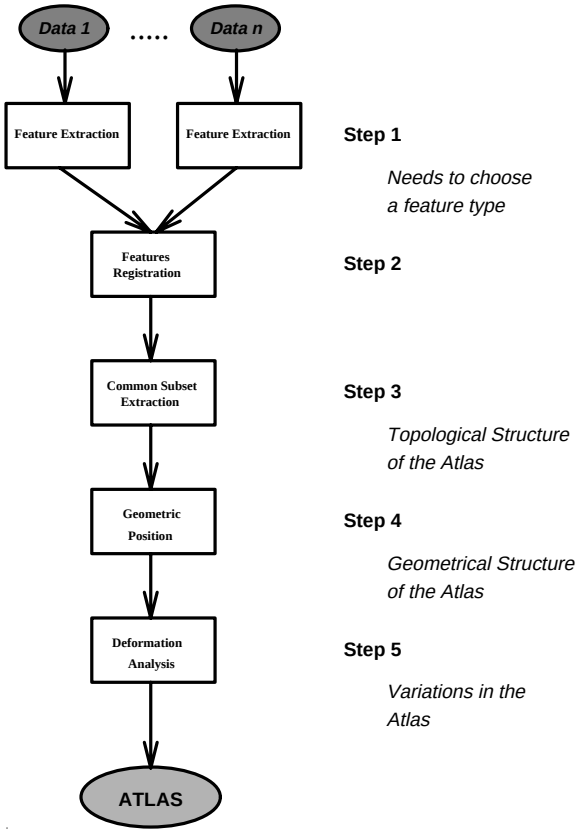

Figure 3: *The proposed general scheme to automatically build anatomical atlases.*

- Step 4: *feature average*. In order to obtain the positions of the features, we "average" the features in each subset, creating the atlas *geometric structure*. We will discuss thoroughly the notion of averaging later on.
- Step 5: *feature deformation analysis*. A statistical process is performed in order to quantify the variations of the features around their average position. This is a key point because such quantitative information is the basis for the atlas applications 5, 6 and 7.

In fact, this scheme is quite close to the manual process where anatomy specialists study several organs in order to find similar structures that they copy out on a paper.

3 Step 1: Feature extraction

We choose to use "crest lines" introduced in [MBF92]. These lines are defined by differential geometry parameters: let k_1 be the principal curvature wich is maximal in absolute value and $\overrightarrow{t_1}$ its associated principal direction, a point P belongs to a crest line when $\overrightarrow{\nabla} k_1 . \overrightarrow{t_1} = 0$ (see Figure 4). The "marching lines" algorithm [TG93] automatically extracts crest lines from the volumetric image.

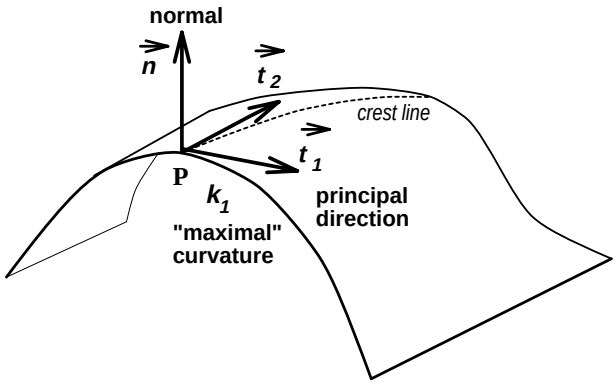

Figure 4: *Differential characteristics of a surface and the crest line.*

Due to their mathematical definition, the crest lines follow the salient lines of a surface. Thus, crest lines of the skull emphasize the mandible, the orbits, the cheekbones or the temples and also, inside the cranium, the sphenoid and temporal bones as well as the occipital foramen (see Figure 5). Such salient structures have been used widely by doctors as anatomical landmarks. For example, crest lines are close to the "ridge lines" presented in [BC88]. On

the brain surface, crest lines follow the convolutions and emphasize some sulci patterns described in the anatomical atlas [OKA90].

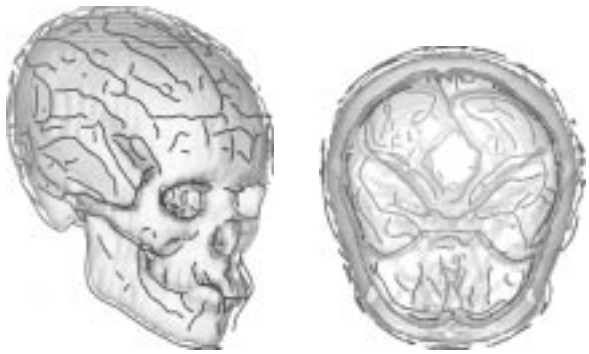

Figure 5: *Crest lines of the skull. Notice the inside lines emphasizing the sphenoid and temporal bones and also the occipital foramen.*

One can argue that such automatically extracted features cannot be anatomically meaningful because, on one hand, of the artefact and noise sensitivity of the automatic process and, on the other hand, of the lack of validation by a specialist as in manual extraction. We answer that in the step 3 of our scheme, we search for the common features and in the steps 4 and 5, we compute statistical information: if no feature is common to all the set or if their variabilities are too great, the features must be rejected. In fact, the general scheme allows us to check the stability of the feature and establish its validity during the atlas building.

Other line features could be used, such as geodesic lines [CBH+93] or lines computed by the 3D Medial Axis Transform [SBK+92]. An atlas can be based also on sparse point features ("extremal points" [Thi93]) or surface features (patches of some differential types [FMPA92]). Of course, the best would be to use both points, lines and surface features as in [CBH+93].

4 Step 2: Features registration

Given two sets of lines extracted from two different patients (see Figure 6), we want a twofold result:

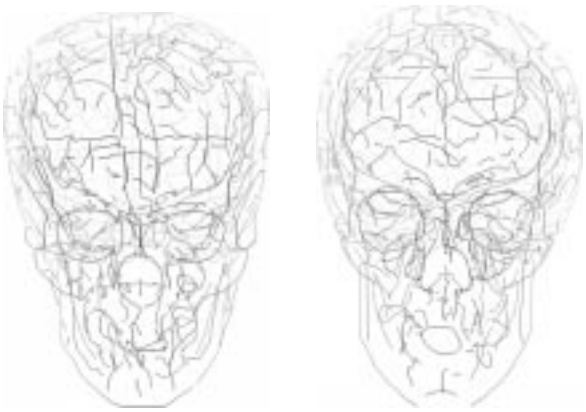

Figure 6: *Two sets of crest lines to register (left $\mathcal{B}$, right $\mathcal{C}$). Notice the difference in size and orientation and the variations in the lines shape, number and discretization. There are 591 lines and 19 302 points in the left set, 583 lines and 19 368 points in the right one.*

- line to line correspondence: the portions $P_{i,k}^{j,l}$ and $P_{j,l}^{'i,k}$, respectively the k^{th} portion of C_i which corresponds to the l^{th} portion of C_j' and vice versa (see Figure 7). This information will be useful for step 3.
- point to point correspondence: those pairs of matched points allow to compute and study the geometry deformations between the sets in the steps 4 and 5.

4.1 The algorithm

As we notice in Figure 6, the sets of lines are very different in orientation, size, number of lines, shape, topology (for example, the sub-mandibular line is

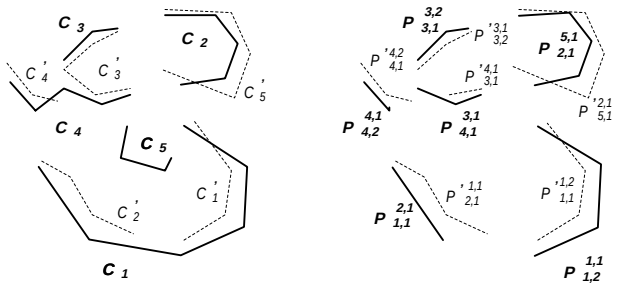

Figure 7: *The registration algorithm has to find the portions $P_{i,k}^{j,l}$ and $P_{j,l}^{'i,k}$, respectively the k^{th} portion of C_i which corresponds to the l^{th} portion of C_j and vice versa.*

in 2 parts on the right and in one part at left) and discretization. Moreover, the data is still complex (several hundreds of lines, thousands of points). Of course the registration is not rigid (translation+rotation) and rules out using curvature based invariants such as proposed in [GA92].

We have adapted "the Iterative Closest Point" algorithm introduced by Besl [BM92] and concurrently by Zhang [Zha92]. The process consists of iteratively applying rigid transformations, based on a local point matching, to the set A in order to superimpose it on the set B. We extend the original method by generalizing it to non-rigid deformations applied to 3D lines.

The algorithm follows four steps described in Figure 8.

At each iteration, the points of the lines of A are linked with their closest neighbour in B according to the Euclidean distance. This gives a first list of couples of registered points. As a line is an *oriented* list of points, we can apply some heuristics to remove non-consistent couples of matched points along the lines in order to define a bijective match between portions of lines.

With this second list of pairs of points, two coefficients are computed: p_i^j and $p_j^{'i}$ which are the proportion of the curve i of A matched with the curve j of B and vice versa. Thus, by thresholding, $p_i^j \geq thr$ and $p_j^{'i} \geq thr$, we can determine the curves "registered" at thr percent. For instance, curves are considered to be definitively registered when $p_i^j \geq 50$ % and $p_j^{'i} \geq 50$ %. In the following, we take into account only the points belonging to lines which are

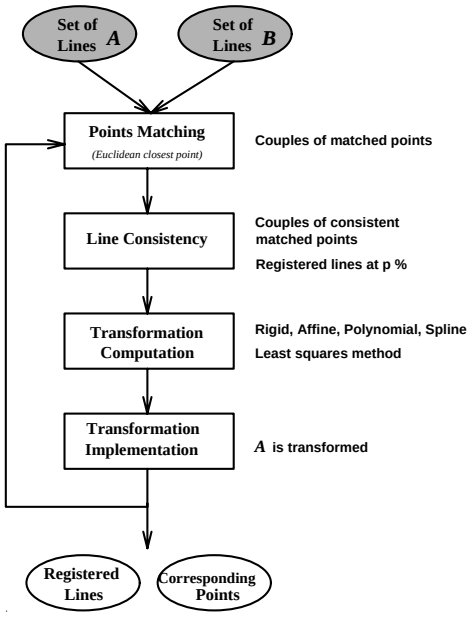

Figure 8: *The features registration algorithm.*

already registered with a given percentage threshold. Raising this threshold as iterations are processed tends to improve the registration of already quite well registered curves.

From this new subset of matched points, we can compute by a least-squares [PFTV88] a transformation T of a given type. We use first rigid transformations in order to align the two sets, then affine transformations to retrieve the scales, quadratic transformations to model some natural deformations [GBHE91] or 3D spline transformations. The spline transformations, detailed in [DSJPA95], allow local deformations but are controlled by a smoothing term based on a second order Tikhonov stabilizer.

The transformation T is then applied to A, bringing A closer to B. We iterate the process, modifying at each step, the threshold on the registration parameter *thr* (for example from 0 % to 50 %) and the type of the transforma-

tion T (for example, five rigid tranformations followed by five affine one and ten spline with a diminishing smoothing parameter).

At the end, we obtain two results: the registered lines by thresholding the registration parameters p_i^j and $p_j^{'i}$ and the matched points belonging to the registered lines.

Despite its simplicity and generality, this algorithm appears quite robust and is quite insensitive to discretization differences (for more details, see [STA94]).

4.2 A practical example

In this example, we register $\mathcal{C}$ towards $\mathcal{B}$. The algorithm takes about 10 minutes on a DEC-Alpha workstation and gives the results displayed in the Figure 9.

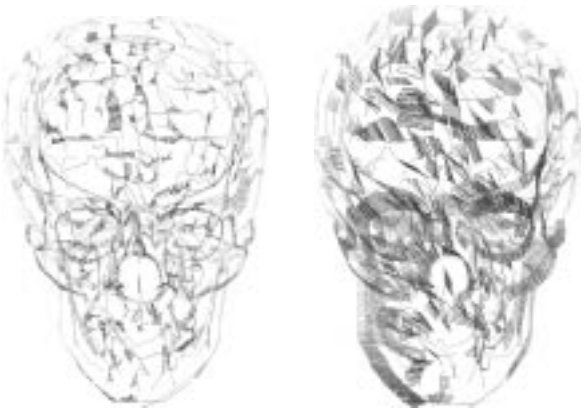

Figure 9: *Registration of $\mathcal{C}$ towards $\mathcal{B}$. Left, we see the deformed set $\mathcal{C}$ with $\mathcal{B}$. The matched points are linked. Notice how the two sets are well superimposed. Right, $\mathcal{C}$ is in its original position. It allows to estimate the extent of the deformation between the two sets.*

We can also plot a graph of the distribution of the matched points distance in Figure 10. At the beginning of the process, for 4 454 couples of points, the mean value is 5.16, and at the end, for 5 999 couples of points (+35%), the

mean value is 2.30 (-55%). It proves the good superimposition of the two sets, generating accurate matched points.

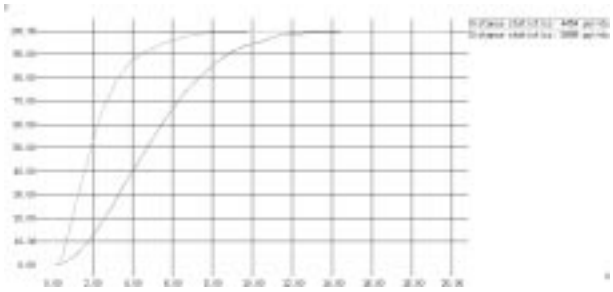

Figure 10: *The graph of the distribution of the distance between matched points belonging to registered lines. Right: at the beginning of the process, for 4 454 couples of points, the mean value is 5.16, Left at the end, for 5 999 couples of points (+35%), the mean value is 2.30 (-55%).*

4.3 Description of step 2

For step 3, we register two by two the sets of crest lines in a circular order. The registration is performed in both directions ($\mathcal{A}$ towards $\mathcal{B}$ and $\mathcal{B}$ towards $\mathcal{A}$) to remove non-symmetric results for registered lines.

For step 4, we register the set $\mathcal{A}$ which will be the reference set with all the others. With the couples of matched points, we can compute by a least

squares method the rigid and homothetic transformations between $\mathcal{A}$ and the other sets.

Summary of step 2:

- Register $\mathcal{A}$ and $\mathcal{B}$, $\mathcal{B}$ and $\mathcal{C}$, $\mathcal{C}$ and $\mathcal{D}$, $\mathcal{D}$ and $\mathcal{E}$, $\mathcal{E}$ and $\mathcal{F}$, $\mathcal{F}$ and $\mathcal{A}$, in both directions. Find the registered lines.
- Register $\mathcal{A}$ with $\mathcal{B}$, $\mathcal{C}$, $\mathcal{D}$, $\mathcal{E}$, $\mathcal{F}$. With the couples of matched points, find the rigid and homothetic transformations.

5 Step 3: Common feature subset extraction

From the registered lines, we are able to build a topological graph where a node is a line of a set and an oriented link represents the relation "is registered with" (see Figure 11).

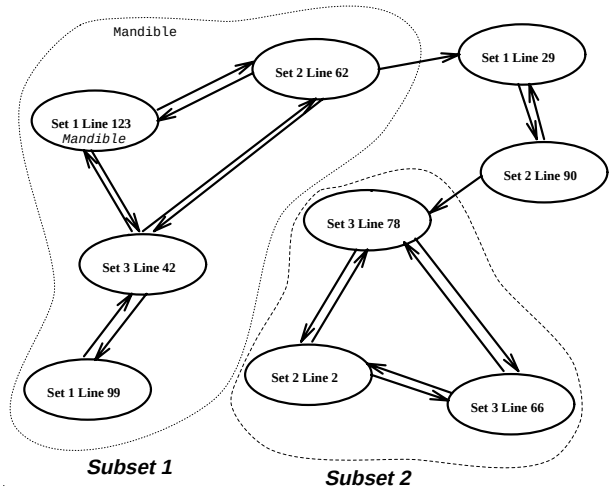

Figure 11: *The topological graph.*

Then, we can extract the bijective connected parts containing at least one line of each set: they represent the subsets of features common to all the data and form the *topological structure* of the atlas.

Thus, for the 6 skulls, we find 63 subsets of lines. We represent in Figure 12 the lines of the skulls $\mathcal{B}$ and $\mathcal{C}$ which are common: we recognize the mandible, the nose, the orbits, the cheekbones, the temples and the occipital foramen.

If the lines of one set have been labelled, it automatically labels the subset to which they belong and then labels the common lines of the other sets.

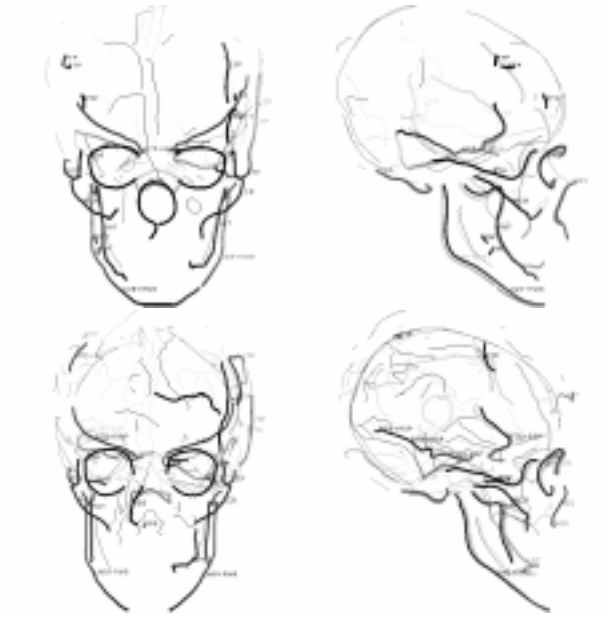

Figure 12: *The topological structure of the atlas is displayed for the skulls $\mathcal{B}$ and $\mathcal{C}$. Some subsets of common lines have been automatically labelled and highlighted: the mandible (bottom and up), the nose, the orbits, the cheekbones, the temples, the occipital foramen and the sphenoid and temporal bones.*

Summary of step 3:

- Build the topological graph.
- Extract the bijective connected parts: the topological structure of the atlas.

6 Step 4: Feature average

Now we have to find the mean positions of the features constituting the atlas i.e. to "average" the sets of 3D lines defining each common subset.

As emphasized in [DL89], in ontogenetic and evolutive shape transformations studies, we are not to take into account differences of size, position and orientation which are not considered as true morphological differences. So, we choose a set of 3D lines as the reference (in our example, the skull $\mathcal{A}$). We invert the global rigid and homothetic transformations between $\mathcal{A}$ and the other data found in the step 3 and we apply them to the other skulls. Now, we have "geometrically normalized" subsets of common lines where the residual deformations between lines are really meaningful differences.

6.1 Modal analysis

Instead of working in the "geometric space" and averaging the positions of points (for example by the method described in [Dea93] and used in [CBH+93]), we study the 3D lines by working in a "deformation space". This space is defined by *modal analysis* introduced in [PS91] and extended in [NA93]. The decomposition in "principal warps" presented in [Boo89] could also be used.

Let $L_A = (M_A^0, M_A^1 \dots M_A^{n-1})$, $L_B = (M_B^0, M_B^1 \dots M_B^{n-1})$ be two matched 3D lines of n points. We can define the deformation between the two lines (for the x coordinate):

$$D_x^{A,B}[i] = (x_{M_B^i} - x_{M_A^i})$$

The formulae of modal analysis allow decomposition of this deformation in the modal basis:

$$d_x^{A,B}[i] = \sum_{p=0}^{n-1} D_x^{A,B}[p].\phi_p[i]$$

where $\phi_p[i] = cos(i\pi(2p-1)/2n)$
Reciprocally, we have:

$$D_x^{A,B}[i] = \sum_{p=0}^{n-1} d_x^{A,B}[p].\phi_p[i]$$

The n parameters $d_x^{A,B}[i]$ are the amplitudes of the basic deformations $\phi_p[i]$, called modes. The first mode represents the translation and rotation of the object. The other modes correspond to more and more complex deformations leaving the center of mass fixed. In Figure 13, we can see the deformation created by the second, the third and the fourth mode applied to a straight line.

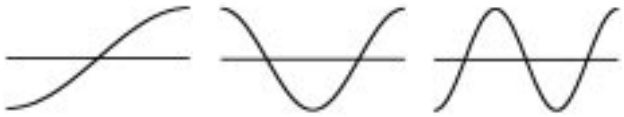

Figure 13: *Deformations of a straight line created by the first mode (left), the second (middle) and the third (right) one. The larger is the mode number, the more complex is the deformation.*

What is particularly interesting in modal analysis is that in the same way as in Fourier analysis, we can approximate a deformation by taking into account just its few first modes. The truncation of the modal development or modal spectrum is a kind of filtering, discarding high frequency deformations. We use this property in order to smooth 3D lines and reduce noise artefacts.

6.2 Description of step 4

For each subset of common lines, thanks to our registration algorithm, we can find the pairs of matched points between the line $L_{\mathcal{A}}$ belonging to the reference set and the lines belonging to $\mathcal{B}$. We create then a deformed $L_{\mathcal{A}}$ called $L_{\mathcal{A},\mathcal{B}}$ by replacing the coordinates of the points of $L_{\mathcal{A}}$ by the coordinates of their correspondent in $\mathcal{B}$. As $L_{\mathcal{A},\mathcal{B}}$ is superimposed on the lines of $\mathcal{B}$, the deformations between $L_{\mathcal{A}}$ and $L_{\mathcal{A},\mathcal{B}}$ represents the gap between the $\mathcal{A}$ and $\mathcal{B}$ common lines subset.

We now study this deformation by modal analysis. We obtain a spectrum $S_{\mathcal{A},\mathcal{B}}$. Similarly, we obtain spectra $S_{\mathcal{A},\mathcal{C}}$, $S_{\mathcal{A},\mathcal{D}}$, $S_{\mathcal{A},\mathcal{E}}$, $S_{\mathcal{A},\mathcal{F}}$ and also $S_{\mathcal{A},\mathcal{A}}$ (which is the null spectrum). Then, as in [SKBG95], we perform an average of the amplitudes of the spectra in order to obtain the mean spectrum S_{mean}. We smooth the deformation D_{mean} associated with S_{mean} by truncation of the spectrum (only 10 % of the amplitudes are kept). Notice that if we have taken the whole average spectrum, it would have been equivalent to averaging the coordinates of the points. We apply D_{mean} to $L_{\mathcal{A}}$ creating the "mean" line.

We present in Figure 14 an example based on the "left orbit" subset. Left, we display the original subset. Right, we discard rigid and homothetic deformations and in black, we present the "mean" left orbit.

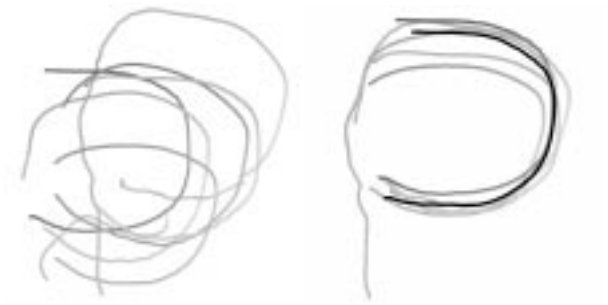

Figure 14: *Left: the original "left orbit" subset. Right: the "mean" left orbit (in black) within the "geometric normalized" subset.*

Summary of step 4:

- Normalize the data $\mathcal{B}$, $\mathcal{C}$, $\mathcal{D}$, $\mathcal{E}$ and $\mathcal{F}$ according to the reference data $\mathcal{A}$ by discarding the rigid and homothetic transformation.
- For each subset of common lines S_i:
  - Deform the line $L_{\mathcal{A}}$ towards the lines of $\mathcal{B}$, $\mathcal{C}$, $\mathcal{D}$, $\mathcal{E}$ and $\mathcal{F}$ belonging to S_i.
  - Compute the modal spectra of $D^{\mathcal{A},\mathcal{B}}$, $D^{\mathcal{A},\mathcal{C}}$, $D^{\mathcal{A},\mathcal{D}}$, $D^{\mathcal{A},\mathcal{E}}$, $D^{\mathcal{A},\mathcal{F}}$, $D^{\mathcal{A},\mathcal{A}}$ in the modal basis.
  - Compute the average modal spectrum and truncate it in order to smooth the resulting average deformation D_{mean}.
  - Apply the deformation D_{mean} to the reference line $L_{\mathcal{A}}$ in order to obtain the mean line L_{mean}.
- All the mean lines constitute the *geometric structure* of the atlas.

6.3 Some results

In Figure 15, we display the set of averaged lines of the atlas. With a spline based technique described in [DSJPA95], we warp the surface of the skull $\mathcal{A}$ according to the registration between its lines and the atlas lines in order to obtain the surface representation of the average skull which is displayed at the beginning of the paper (Figure 2).

We notice three things:

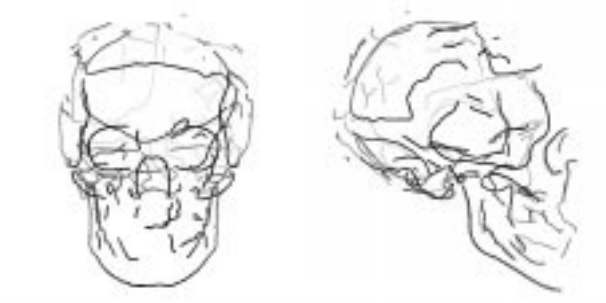

Figure 15: *The average lines of the atlas. Notice the symmetry in the lateral view.*

- the atlas is symmetric whereas the averaging process is independent for each subset of common lines. Thus, it shows that the algorithm is consistent.
- the reference set $\mathcal{A}$ was very dolichocephalic (longer than wider head with a narrow face) whereas the five other skulls are more brachycephalic (more round head). The atlas is more brachycephalic so it proves that the averaging process has correctly taken into account the data of the other skulls.
- our atlas is visually very similar to the one presented in [CBH+93].

7 Step 5: Feature deformations analysis

7.1 The algorithm

Deformation analysis is a key step in order to contrast healthy and affected organic structures. We are going to use modal decomposition as in [NA94] (application to cardiac deformations) and [MPK94] (shape analysis of brain structures).

By the same process as in step 4 (just replacing $\mathcal{A}$ by the atlas), we register the features of the atlas and of the data in order to find deformations in the

"geometric normalized" frame. We compute the spectra of these deformations. We can then deduce some statistics for each amplitude i, in particular its mean value d_i (which is very close to 0) and its standard deviation σ_i.

We define two distances, which can be computed for the axis x, y or z:

- a *global distance* to estimate how important a deformation $D^{atlas,B}$ is, and then, moves away B from the atlas. This distance measures the sum of all the modal amplitudes of the deformation:

$$dist_{glob}(D^{Atlas,B}) = \frac{1}{n}\sqrt{\sum_{i=1}^{n} \frac{(d^{atlas,B}[i] - d_i)^2}{\sigma_i^2}}$$

  With $dist_{glob}(D^{Atlas,B})$, we can estimate if a structure is far from its mean position and if so, it must be considered "abnormal".

- an *amplitude distance*. Nevertheless, the global distance gives only an overview of the intensity of the deformation. To be more precise and to know what is the kind of an "abnormal" deformation, we have to compare each amplitude by:

$$dist_{amp}(D^{Atlas,B}, i) = \sqrt{\frac{(d^{Atlas,B}[i] - d_i)^2}{\sigma_i^2}}$$

  The large $dist_{amp}(D^{Atlas,B}, i)$ enable us to find the modes characterizing the "abnormal" deformation.

7.2 An example

We want to study the axial deformations of the sub-mandibular line. The global distances for the z coordinate between the 6 skulls and the atlas are listed in table I. We notice the high value for the skull $\mathcal{D}$.

Now, let us study the spectrum of the deformation between the atlas and $\mathcal{D}$ by computing the amplitude distances (see table II). It appears that the second and the fourth amplitudes are too large and so, we conclude that the deformations associated with these modes are "abnormal". To visualize the

$\mathcal{A}$	$\mathcal{B}$	$\mathcal{C}$	$\mathcal{D}$	$\mathcal{E}$	$\mathcal{F}$
4.14	8.02	2.38	11.69	2.12	2.51

Table 1: *Global distances for the z coordinate between the 6 skulls and the atlas for the five first modes. Notice the high value of* $\mathcal{D}$.

kind of abnormality, we apply to the mean mandible line of the atlas a deformation with a large value of the 2^{th} and 4^{th} modes whereas the others are null. The result displayed in Figure 16 left, shows that the mandible of $\mathcal{D}$ is too low as it is confirmed when we look at the real skull, right.

Mode 0	Mode 1	Mode 2	Mode 3	Mode 4
1.48	0.05	50.08	1.67	83.38

Table 2: *Amplitude distances for the 5 first modes of the z deformations between the atlas and* $\mathcal{D}$. *The* 2^{nd} *and* 4^{th} *mode can be considered as "abnormal".*

Summary of step 5:

- For each element of the atlas
  - Compute the deformations between the atlas and all the data.
  - Compute the mean value and the standard deviation error for each amplitude of the deformations.
  - These parameters allow to define global and amplitude distances.

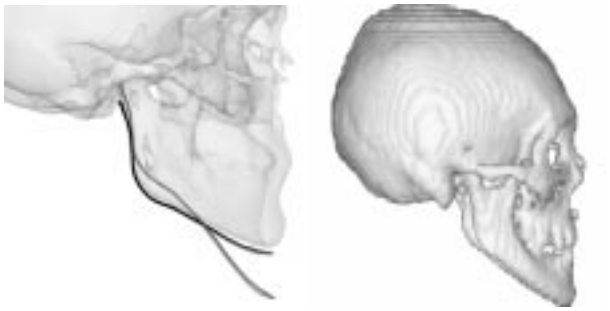

Figure 16: *Left: the mean mandible line of the atlas (in black) has been deformed (in grey) according to the* 2^{nd} *and* 4^{th} *modes. It shows that these latter are characteristic of a wider angle of jaw . We can verify this deformation on the skull* $\mathcal{D}$*, right.*

8 A craniofacial application: Crouzon's disease study

In this section, we use the skull atlas in order to study a skull $\mathcal{CR}$ affected by Crouzon's disease (see Figure 17) which is a congenital craniofacial malformation.

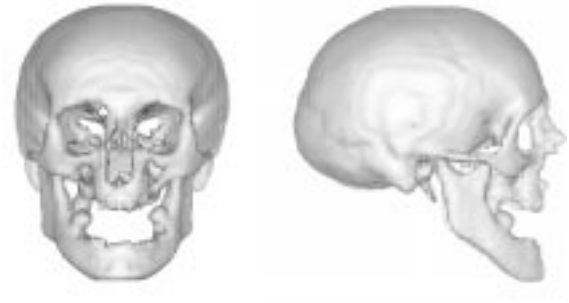

Figure 17: *The skull* $\mathcal{CR}$ *affected by Crouzon's disease.*

8.1 Passive aided surgery

We register the atlas with $\mathcal{CR}$. With the pairs of matched points, we find the rigid and homothetic transformations which we apply to the skull atlas in order to superimpose it on $\mathcal{CR}$ (see Figure 18). In this way, we are able to contrast the two skulls and emphasize the symptoms of Crouzon's disease (precisely described in [KB82]) as, for example, the mandible which is prognathic, the skull shape which is flattened and too large or the orbits which are too large.

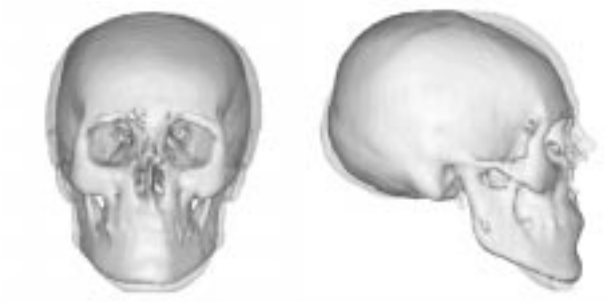

Figure 18: *Rigid and scale registration of the atlas (opaque) with $\mathcal{CR}$ (transparent) emphasizing the symptoms of the Crouzon syndrome as the low mandible, the flattened shape of the skull or the large orbits.*

Moreover, the surgeon could use this superimposed display to estimate his procedures.

8.2 Shape and deformation analysis

Such a normalized registration can only give some qualitative information. In fact, we need a quantitative analysis of the symptoms. Let us analyze the deformations of the mandible of $\mathcal{CR}$. With the method described in the previous section, we compute the 5 first modes of the $\mathcal{CR}$ mandible deformation according to the mean position of the atlas. The results for the three axes are listed in table III. We notice that the 2^{nd} y-mode and the 4^{th} z-mode amplitude distances are very large and these modes can be considered as typical

abnormalities of Crouzon's disease. The amplitude distances could be used to define the severity of the disease.

Axis	Mode 0	Mode 1	Mode 2	Mode 3	Mode 4
x	0.011	5.10	0.011	1.647	0.167
y	0.006	0.019	27.232	0.501	3.150
z	0.035	0.009	4.901	0.584	70.557

Table 3: *Amplitude distances for the 5 first modes of the mandible deformation between the atlas and $\mathcal{CR}$. The 2^{nd} y-mode and 4^{th} z-mode can be considered as "abnormal".*

8.3 A "virtual patient"

In order to estimate the mandible symptom, we can deform the mean mandible of the atlas according to the 2^{th} y-mode and the 4^{th} z-mode. So, with only 2 coefficients, we are able to deform the atlas mandible towards a pathological case. By using the warping algorithm cited in step 4, we can create a "normal" skull with a mandible affected by a severe Crouzon's disease: the jaw is now prognathic (see Figure 19).

9 Conclusion

In this paper, we have shown how an entirely automatic process can lead to a precise and quantitative anatomical atlas. We have presented initial results for a skull atlas based on 6 CT-Scan images of different patients. With such an atlas, it becomes possible to consider new applications such as performing an automatic diagnosis. We have obtained preliminary results about automatic contrasting the skull atlas with a skull affected by Crouzon's disease.

Figure 19: *The mandible of the atlas has been deformed according to only 2 values characterizing the symptoms of Crouzon's disease.*

The described scheme is quite general and could be applied to crest lines of the brain or 3D skeletons of vascular networks.

We thank General-Electric and Bruce Latimer, Director at the Cleveland Museum of Natural History, Court Cutting, David Dean and André Guéziec for the CT-Scan data of the skulls. This work was partially supported by DEC. We want to thank Mike Brady, Jérôme Declerck and Jacques Feldmar for their substantial help.

References

[BBW+94] Jennifer L. Boes, Peyton H. Bland, Terry E. Weymouth, Leslie E. Quint, Fred L. Bookstein, and Charles R. Meyer. Generating a Normalized Geometric Liver Model Using Warping. *Investigative Radiology*, 29(3):281–286, 1994.

[BC88] Fred L. Bookstein and Court B. Cutting. A proposal for the apprehension of curving cranofacial form in three dimensions. In K. Vig and A. Burdi, editors, *Cranofacial Morphogenesis and Dysmorphogenesis*, pages 127–140. 1988.

[BFAD95] F. Betting, J. Feldmar, N. Ayache, and F. Devernay. A new framework for fusing stereo images with volumetric medical images. In Nicholas Ayache, editor, *CVRMed'95*, volume 905 of *Lecture Notes in Computer Science*, pages 30–39, Nice (France), April 1995. Springer-Verlag.

[BGM+94] C. Barillot, N.B. Gibaud, E. Montabord, S. Garlatti, N. Gauthier, and I. Kanellos. An information system to manage anatomical knowledge and image data about brain. In Richard A. Robb, editor, *Visualization in Biomedical Computing*, volume 2359 of *SPIE*, pages 424–434, Rochester (Minnesota) (USA), October 1994.

[BK89] Ruzena Bajcsy and Stane Kovačič. Multiresolution Elastic Matching. *Computer Vision, Graphics and Image Processing*, (46):1–21, 1989.

[BM92] Paul J. Besl and Neil D. McKay. A Method for Registration of 3-D Shapes. *IEEE PAMI*, 14(2):239–255, February 1992.

[Boo89] Fred L. Bookstein. Principal Warps: Thin-Plate Splines and the Decomposition of Deformations. *IEEE Transactions on Pattern Analysis and Machine Intelligence*, 11(6):567–585, June 1989.

[Boo91] Fred L. Bookstein. *Morphometric tools for landmark data.* Cambridge University Press, 1991.

[CBH+93] Court B. Cutting, Fred L. Bookstein, Betsy Haddad, David Dean, and David Kim. A spline-based approach for averaging three-dimensional curves and surfaces. In David C. Wilson and Joseph N. Wilson, editors, *Mathematical Methods in Medical Imaging II 1993*, pages 29–44, San Diego, California (USA), July 1993. SPIE.

[CMV94] Gary E. Christensen, Michael I. Miller, and Michael Vannier. A 3D Deformable Magnetic Resonance Textbook Based on Elasticity. In *Applications of Computer Vision in Medical Image*

Processing, pages 153–156, Stanford University (USA), March 1994.

[CZH+94] A.C.F. Colchester, J. Zhao, C. Henri, R.L. Evans, P. Roberts, N. Maitland, D.J. Hawkes, D.L.G. Hill, A.J. Strong, D.G. Thomas, M.J. Gleeson, and T.C.S. Cox. Craniotomy Simulation and Guidance using a Stereo Video Based Tracking System (VISLAN). In Richard A. Robb, editor, *Visualization in Biomedical Computing*, volume 2359 of *SPIE*, pages 541–551, Rochester, Minnesota (USA), October 1994.

[Dea93] David Dean. *The Middle Pleistocene Homo erectus/Homo sapiens Transition: New Evidence from Space Curve Statistics.* PhD thesis, The City University of New York, 1993.

[DL89] Bruno David and Bernard Laurin. Déformations ontogénétiques et évolutives des organismes : l'approche par la méthode des points homologues. *C. R. Académie des Sciences Paris*, II(309):1271–1276, 1989.

[DSCP94] Hervé Delingette, Gérard Subsol, Stéphane Cotin, and Jérôme Pignon. A Craniofacial Surgery Simulation Testbed. Technical Report 2199, INRIA, February 1994.

[DSJPA95] Jérôme Declerck, Gérard Subsol, Thirion Jean-Philippe, and Nicholas Ayache. Automatic retrieval of anatomical structures in 3D medical images. In Nicholas Ayache, editor, *CVRMed'95*, volume 905 of *Lecture Notes in Computer Science*, pages 153–162, Nice (France), April 1995. Springer Verlag.

[FMPA92] Denis Friboulet, Isabelle E. Magnin, Andreas Pommert, and Michel Amiel. 3D Curvature Features of the Left Ventricle from CT Volumic Images. In *Information Processing in Medical Imaging*, pages 182–192. IPMI'92, 1992.

[GA92] A. Guéziec and N. Ayache. Smoothing and Matching of 3-D Space Curves. In *Visualization in Biomedical Computing*, pages

259–273, Chapel Hill, North Carolina (USA), October 1992. SPIE.

[GBHE91] Torgny Greitz, Christian Bohm, Sven Holte, and Lars Eriksson. A Computerized Brain Atlas: Construction, Anatomical Content and Some Applications. *Journal of Computer Assisted Tomography*, 15(1):26–38, 1991.

[GLPWI+94] W.E.L. Grimson, T. Lozano-Pérez, W.M. Wells III, G.J. Ettinger, S.J. White, and R. Kikinis. An Automatic Registration Method for Frameless Stereotaxy, Image Guided Surgery, and Enhanced Reality Visualization. In *CVPR'94*, pages 430–436, Seattle, Washington (USA), June 1994.

[GRB93] Jim C. Gee, Martin Reivich, and Ruzena Bajcsy. Elastically Deforming 3D Atlas to Match Anatomical Brain Images. *Journal of Computer Assisted Tomography*, 17(2):225–236, March 1993.

[Har94] T. L. Hardy. Computerized atlas for functional stereotaxis robotics and radiosurgery. In Richard A. Robb, editor, *Visualization in Biomedical Computing*, volume 2359 of *SPIE*, pages 447–456, Rochester (Minnesota) (USA), October 1994.

[HBR+92] Karl Heinz Höhne, Michael Bomans, Martin Riemer, Rainer Schubert, Ulf Tiede, and Werner Lierse. A Volume-based Anatomical Atlas. *IEEE Computer Graphics & Applications*, pages 72–78, July 1992.

[KB82] Sven Kreiborg and Arne Björk. Description of a Dry Skull with Crouzon Syndrome. *Scandinavian Journal of Plastic and Reconstructive Surgery*, 16(3):245–253, 1982.

[LTG+92] S. Lavallée, J. Troccaz, L. Gaborit, P. Cinquin, A.L. Benabid, and D. Hoffmann. Image guided operating robot: a clinical application in stereotactic neurosurgery. In *International Conference on Robotics and Automation*, volume 1, pages 618–624. IEEE, May 1992.

[MBF92] Olivier Monga, Serge Benayoun, and Olivier D. Faugeras. Using Partial Derivatives of 3D Images to Extract Typical Surface Features. In *CVPR*, 1992.

[MDB+94] O. Migneco, J. Darcourt, J. Benoliel, F. Martin, Ph. Robert, F. Bussiere-Lapalus, and I. Mena. Computerized localization of brain structures in single photon emission computed tomography using a proportional anatomical stereotactic atlas. *Computerized Medical Imaging and Graphics*, 18(6):413–422, 1994.

[MECP89] S. Marrett, A. C. Evans, L. Collins, and T. M. Peters. A Volume of Interest (VOI) Atlas for the Analysis of Neurophysiological Image Data. In *Medical Imaging III: Image Processing*, volume 1092, pages 467–477. SPIE, 1989.

[MFB+94] Jean-François Mangin, Vincent Frouin, Isabelle Bloch, Jean Régis, and Jaime López-Krahe. Automatic construction of an attributed relational graph representing the cortex topography using homotopic transformations. In *SPIE, Mathematical Methods in Medical Imaging III*, San-Diego (USA), July 1994.

[MPK94] John Martin, Alex Pentland, and Ron Kikinis. Shape Analysis of Brain Structures Using Physical and Experimental Modes. In *Applications of Computer Vision in Medical Image Processing*, pages 110–113, Stanford University (USA), March 1994.

[NA93] Chahab Nastar and Nicholas Ayache. Non-Rigid Motion Analysis in Medical Images: A Physically Based Approach. In *Information Processing in Medical Imaging*, Flagstaff, Arizona (USA), June 1993. IPMI.

[NA94] Chahab Nastar and Nicholas Ayache. Classification of Nonrigid Motion in 3D Images using Physics-Based Vibration Analysis. In *IEEE Workshop on Biomedical Analysis*, pages 61–69, Seattle (USA), June 1994.

[NFN+95] W.L. Nowinski, A. Fang, B.T. Nguyen, R. Raghavan, R.N. Bryan, and J. Miller. Talairach-Tournoux / Schaltenbrand-Wahren Based Electronic Brain Atlas System. In Nicholas Ayache, editor, *CVRMed'95*, volume 905 of *Lecture Notes in Computer Science*, pages 257–261, Nice (France), April 1995. Springer Verlag.

[Nig90] Jörg Niggemann. Analysis and representation of neuroanatomical knowledge. *Applied Artificial Intelligence*, 4:309–336, 1990.

[OISJ+95] R.V. O'Toole III, D.A. Simon, B. Jaramaz, O. Ghattas, M.K. Blackwell, L. Kallivokas, F. Morgan, C. Visnic, A.M. DiGioia III, and T. Kanade. Towards More Capable and Less Invasive Robotic Surgery in Orthopaedics. In Nicholas Ayache, editor, *CVRMed'95*, volume 905 of *Lecture Notes in Computer Science*, pages 123–130, Nice (France), April 1995. Springer-Verlag.

[OKA90] Michio Ono, Stefan Kubik, and Chad D. Abernathey. *Atlas of the Cerebral Sulci*. Georg Thieme Verlag, 1990.

[Per83] Eduard Pernkopf. *Atlas d'anatomie humaine*. Piccin, 1983.

[PFTV88] William H. Press, Brian P. Flannery, Saul A. Teukolsky, and William T. Vettening. *Numerical Recipes in C, The Art of Scientific Computing*. Cambridge University Press, 1988.

[PS91] Alex Pentland and Stan Sclaroff. Closed-Form Solutions for Physically Based Shape Modeling and Recognition. *IEEE Transactions on Pattern Analysis and Machine Intelligence*, 13(7):715–729, July 1991.

[PSR+94] A. Pommert, R. Schubert, M. Riemer, T. Schiemann, U. Tiede, and K. H. Höhne. Symbolic Modeling of Human Anatomy for Visualization and Simulation. In Richard A. Robb, editor, *Visualization in Biomedical Computing*, volume 2359 of *SPIE*, pages 412–423, Rochester, Minnesota (USA), October 1994.

[SBK+92] G. Székely, Ch. Brechbühler, O. Kübler, R. Ogniewicz, and T. Budinger. Mapping the human cerebral cortex using 3D medial manifolds. In Richard A. Robb, editor, *Visualization in Biomedical Computing*, pages 130–144, Chapel Hill, North Carolina (USA), October 1992. SPIE.

[SHC+94] Thomas Schiemann, Karl Heinz Höhne, Koch Christoph, Pommert Andreas, Martin Riemer, Rainer Schubert, and Ulf Tiede. Interpretation of Tomographic Images Using Automatic Atlas Lookup. In Richard A. Robb, editor, *Visualization in Biomedical Computing*, volume 2359 of *SPIE*, pages 457–465, Rochester (Minnesota) (USA), October 1994.

[SKBG95] G. Székely, A. Kelemen, Ch. Brechbühler, and G. Gerig. Segmentation of 3D Objects from MRI Volume Data Using Constrained Elastic Deformations of Flexible Fourier Surface Models. In Nicholas Ayache, editor, *CVRMed'95*, volume 905 of *Lecture Notes in Computer Science*, pages 495–505, Nice (France), April 1995. Springer-Verlag.

[STA94] Gérard Subsol, Jean-Philippe Thirion, and Nicholas Ayache. First Steps Towards Automatic Building of Anatomical Atlases. Technical Report 2216, INRIA, March 1994.

[SYMK95] Hidetomo Suzuki, Keiichi Yoshizaki, Michimasa Matsuo, and Jiro Kashio. A Supporting System for Getting Tomograms and Screening with a Computerized 3D Brain Atlas and a Knowledge Database. In Nicholas Ayache, editor, *CVRMed'95*, volume 905 of *Lecture Notes in Computer Science*, pages 170–176, Nice (France), April 1995. Springer Verlag.

[Tay93] Russel H. Taylor. An Overview of Computer Assisted Surgery Research at IBM T. J. Watson Research Center. In *Sixth International Symposium on Robotics Research*, Hidden Valley, PA (USA), October 1993. ISRR.

[TG93] J.P. Thirion and A. Gourdon. The Marching Lines Algorithm : new results and proofs. Technical Report 1881, INRIA, March 1993.

[Thi93] J.P. Thirion. New feature points based on geometric invariants for 3D image registration. Technical Report 1901, INRIA, May 1993.

[TSLA95] R. Tombropoulos, A. Schweikard, J.-C. Latombe, and J. Adler. Treatment Planning for Image-Guided Robotic Radiosurgery. In Nicholas Ayache, editor, *CVRMed'95*, volume 905 of *Lecture Notes in Computer Science*, pages 131–137, Nice (France), April 1995. Springer-Verlag.

[Zha92] Zhengyou Zhang. On Local Matching of Free-Form Curves. In David Hogg and Roger Boyle, editors, *British Machine Vision Conference*, pages 347–356, Leeds (United Kingdom), September 1992. British Machine Vision Association, Springer-Verlag.

Unité de recherche INRIA Lorraine, Technopôle de Nancy-Brabois, Campus scientifique,
615 rue du Jardin Botanique, BP 101, 54600 VILLERS LÈS NANCY
Unité de recherche INRIA Rennes, Irisa, Campus universitaire de Beaulieu, 35042 RENNES Cedex
Unité de recherche INRIA Rhône-Alpes, 46 avenue Félix Viallet, 38031 GRENOBLE Cedex 1
Unité de recherche INRIA Rocquencourt, Domaine de Voluceau, Rocquencourt, BP 105, 78153 LE CHESNAY Cedex
Unité de recherche INRIA Sophia-Antipolis, 2004 route des Lucioles, BP 93, 06902 SOPHIA-ANTIPOLIS Cedex

Éditeur
INRIA, Domaine de Voluceau, Rocquencourt, BP 105, 78153 LE CHESNAY Cedex (France)
ISSN 0249-6399